JACS
JOURNAL OF THE AMERICAN CHEMICAL SOCIETY
Article
pubs.acs.org/JACS

# Phase Transformation and Lithiation Effect on Electronic Structure of $Li_xFePO_4$: An In-Depth Study by Soft X-ray and Simulations

Xiaosong Liu,[†] Jun Liu,[‡] Ruimin Qiao,[†,∥] Yan Yu,[¶] Hong Li,[#] Liumin Suo,[#] Yong-sheng Hu,[#] Yi-De Chuang,[†] Guojiun Shu,[⊥] Fangcheng Chou,[⊥] Tsu-Chien Weng,[△] Dennis Nordlund,[△] Dimosthenis Sokaras,[△] Yung Jui Wang,[×] Hsin Lin,[×] Bernardo Barbiellini,[×] Arun Bansil,[×] Xiangyun Song,[‡] Zhi Liu,[†] Shishen Yan,[∥] Gao Liu,[‡] Shan Qiao,[⊗] Thomas J. Richardson,[‡] David Prendergast,[§] Zahid Hussain,[†] Frank M. F. de Groot,[▽] and Wanli Yang*[,†]

[†]Advanced Light Source, [‡]Environmental Energy Technologies Division, and [§]The Molecular Foundry, Lawrence Berkeley National Laboratory, Berkeley, California 94720, United States

[∥]School of Physics, Shandong University, Jinan, Shandong, 250100, China

[¶]Max Planck Institute for Solid State Research, Stuttgart 70569, Germany

[#]Institute of Physics, Chinese Academy of Sciences, Beijing, 100080, China

[⊥]Center for Condensed Matter Sciences, National Taiwan University, Taipei, 10617 Taiwan

[△]Stanford Synchrotron Radiation Lightsource, SLAC National Accelerator Laboratory, Menlo Park, California 94025, United States

[×]Department of Physics, Northeastern University, Boston, Massachusetts 02115, United States

[⊗]Laboratory of Advanced Materials, Department of Physics, Fudan University, Shanghai, 200438, China

[▽]Department of Chemistry, Utrecht University, 3584 CA Utrecht, The Netherlands

Supporting Information

**ABSTRACT:** Through soft X-ray absorption spectroscopy, hard X-ray Raman scattering, and theoretical simulations, we provide the most in-depth and systematic study of the phase transformation and (de)lithiation effect on electronic structure in $Li_xFePO_4$ nanoparticles and single crystals. Soft X-ray reveals directly the valence states of Fe 3d electrons in the vicinity of Fermi level, which is sensitive to the local lattice distortion, but more importantly offers detailed information on the evolution of electronic states at different electrochemical stages. The soft X-ray spectra of $Li_xFePO_4$ nanoparticles evolve vividly with the (de)lithiation level. The spectra fingerprint the (de)lithiation process with rich information on Li distribution, valency, spin states, and crystal field. The high-resolution spectra reveal a subtle but critical deviation from two-phase transformation in our electrochemically prepared samples. In addition, we performed both first-principles calculations and multiplet simulations of the spectra and quantitatively determined the 3d valence states that are completely redistributed through (de)lithiation. This electronic reconfiguration was further verified by the polarization-dependent spectra collected on $LiFePO_4$ single crystals, especially along the lithium diffusion direction. The evolution of the 3d states is overall consistent with the local lattice distortion and provides a fundamental picture of the (de)lithiation effects on electronic structure in the $Li_xFePO_4$ system.

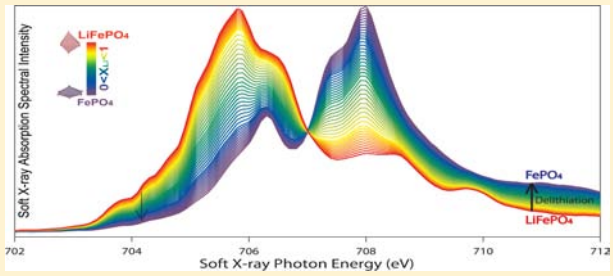


## INTRODUCTION

Li-ion batteries, the most promising power source for electric vehicles, are revolutionizing the transportation technology by reducing the dependence on fossil oil and decreasing the carbon footprint. Besides energy and power densities, safety is critical for the transportation application of Li-ion batteries.[1−3] Olivine-structured $LiFePO_4$ offers a safe operation based on the fundamental electronic structure of the Fe 3d and O 2p states as well as the high interfacial and thermal stability.[4,5] In addition, olivine $LiFePO_4$ can provide impressive high-rate performance.[6] However, how $LiFePO_4$, a poor electronic and ionic conductor, could offer a facile (de)lithiation during battery operation remains an active topic[6−13] and challenges our conventional wisdom on choosing and developing cathode materials.

Charge/discharge (delithiation/lithiation) of olivine $LiFePO_4$ is a two-phase transition reaction, which has been extensively verified through structural probes.[14−16] Nevertheless, Chen et al. have revealed a phase "transition zone" with TEM and suggested that Li-ions diffuse along such transition phase with the boundary progresses perpendicularly.[8]

Received: April 18, 2012
Published: July 26, 2012

   dx.doi.org/10.1021/ja303225e | J. Am. Chem. Soc. 2012, 134, 13708−13715

The very recent annular bright-field (ABF) electron microscopy shows an intriguing staging phase, i.e., a single phase, in partially delithiated $Li_xFePO_4$,[17] which also tends to exist at the phase boundary.[18] More strikingly, theoretical studies suggest that the $LiFePO_4$ system could circumambulate the energy barrier for a two-phase process by going through such a metastable single phase.[11] In the meantime, the vast experimental results do support the two-phase model, e.g., refs 14−16, indicating that such a critical nonequilibrium single phase, if it exists, is only in a finite amount/size. Above all, the single phase with an ordered lithium distribution essentially maintains the (Li)$FePO_4$ local structure,[17,18] and the small size intrinsically broadens features in the X-ray diffraction (XRD) studies; thus it is unclear whether such a phase should exhibit structural distinction at all. Therefore, in addition to the structural probes, it becomes crucial to develop new approaches for investigating the subtle effect on *nonstructural* properties related to this controversial phase transformation issue.

Another renowned feature of $LiFePO_4$ system is its high anisotropy on both lithium diffusion and electron conductivity. Theoretical[19,20] and experimental[10,21] results have verified that lithium diffuses in $LiFePO_4$ along a particular one-dimensional chain. In parallel, electric conductivity also exhibits a certain level of anisotropy.[22] Because the small polaron, the quasi-particle formed by the charge carrier and its self-induced local lattice distortion, determines the electron conduction in $LiFePO_4$ and $FePO_4$,[9,13,23,24] the anisotropy on electronic structure is coupled to the local structure and will play an important role in defining both electron and Li-ion conductivity. Indeed, Mössbauer results by Ellis et al.[9] suggested strong coupling between electron and lithium transport. Experimentally, such anisotropic electronic structure has only been studied indirectly by hard X-ray absorption spectroscopy (XAS),[25] where the key Fe 3d states are accessed through the weak dipole-forbidden 1s→3d quadrupole transitions and do not manifest fine details in the 3d states.

From a fundamental point of view, it is intriguing that a facile electrochemical process could take place in a two-phase system with localized polarons. The fundamental electronic structure has thus been extensively studied theoretically within the framework of density functional theory (DFT).[26−30] The theoretical calculations have predicted much of the dynamics of the lithiation process[11,12,20,23,31] and delivered fairly detailed information of the density of states (DOS) with emphasis on the transition metals in olivine cathode materials.[24,27,29,30,32] It is demonstrated that DFT+U method is required to correctly predict the band gap, due to the very localized character on 3d orbitals in the olivine phosphate compounds.[29,30] Recently, a first-principles calculation indicated that both Li mobility and electron (polaron) conductivity are significantly enhanced by the local structure change.[32] The result showed the critical effects of the local crystal structure changes on the electronic structure and, consequently, the kinetic and thermodynamic properties of olivine cathodes. Such strong correlation between the local lattice structure and the electronic structure could be directly resolved through soft XAS, as demonstrated in this work.

Experimentally, the electronic structure of $Li_xFePO_4$ has been studied by electron energy loss spectroscopy (EELS),[15,33−35] X-ray photoelectron spectroscopy (XPS),[36] soft X-ray absorption and emission spectroscopy,[37−40] and hard X-ray absorption.[25,41] Although these spectroscopic results presented various electronic properties, such as the Fe valency and the DOS for particular purposes, they lacked either the high resolution for revealing the detailed electronic states modified by the local lattice distortion or the intermediate states for studying the phase transformation issues.

In this article, we try to tackle all the aforementioned issues through a detailed study on a series of chemically delithiated $Li_xFePO_4$ nanorods, electrochemically cycled $Li_xFePO_4$ cathodes with the Li staging phase,[17] and large $LiFePO_4$ single crystals. We have focused on high-resolution Fe-L edge soft XAS, and hard X-ray Raman scattering (XRS), which directly depicts the evolution of the electronic properties of Fe 3d states in $Li_xFePO_4$. The spectra with abundant features enabled detailed studies on the subtle effects related to the two-phase issue in the intermediate states. The (de)lithiation level, the anisotropic effect, and the configuration of Fe 3d electronic structure are determined through the combination of high-quality spectroscopic data with DFT+U theoretical calculations and multiplet simulations.

## TECHNICAL SECTION

**Sample Preparation.** Chemically delithiated $Li_xFePO_4$ ($0 < x < 1$) samples, denoted as S#, were prepared by stirring $LiFePO_4$ in suitable amount of 0.05 M solution of bromine in acetonitrile for 3 h. The TEM images and XRD patterns at different lithiation levels are presented in Supporting Information. Samples were kept in a glovebox for more than half of a year before measurements. Electrochemically cycled $LiFePO_4$ samples, denoted as EC#, were prepared and characterized as described in ref 17. The ABF electron microscope has detected the existence of an intermediate ordered in these samples,[17] which may be the key to understand the puzzling performance of $LiFePO_4$ system.[11] Considering the possible metastable feature of such a phase, in this work, we perform the spectroscopic experiments within the same time scale as that for the ABF electron microscope measurements, i.e., one week after the sample preparation, through an efficient international collaboration. $LiFePO_4$ single crystals were grown using an optical floating zone method under argon gas environment. The nearly stoichiometric feed rod was melted, recrystallized, and grown into a large single crystal. The XRD patterns are presented in Supporting Information.

**Soft X-ray Absorption Spectroscopy.** The Fe *L*-edge XAS spectroscopy was performed at the undulator beamline 8.0 of the Advanced Light Source (ALS) at Lawrence Berkeley National Laboratory (LBNL) with resolving power up to 6000. The spectra were collected in both total electron yield (TEY) and total fluorescence yield (TFY) modes with the data normalized to the photon flux of incident beam. The experimental resolution is about 0.12 eV at the Fe *L*-edge without considering the core−hole broadening effect. Only TEY data from soft X-ray measurements are shown here because it has very recently been demonstrated that the TFY line shape is not very reliable for detailed analysis in cathode materials without high-*Z* elements.[42] To avoid the oxidation effect on the samples, all samples were prepared in the Ar glovebox, sealed in Ar bags for transportation, and transferred through a $N_2$ glovebag into our ultrahigh-vacuum experimental endstation to minimize the exposure to the air. The bulk probe was accessed by hard XRS.

**Hard X-ray Raman Scattering.** Because of the shallow probe depth of soft X-ray spectroscopy, especially in the TEY mode, we performed hard XRS on the same set of samples. Measurements were carried out with the 40 element XRS spectrometer of beamline 6-2 at Stanford Synchrotron Radiation Lightsource (SSRL).[43] Within the low-momentum transfer regime, the cross-section of hard XRS is dominated by dipole transitions and thus provides identical information to soft XAS. Although with much lower statistics, the XRS data (measured with the Si-660 reflection of the XRS spectrometer, which corresponds to an incident scanning energy of about 10.4 keV) show unambiguously that the fine structures in the


dx.doi.org/10.1021/ja303225e | J. Am. Chem. Soc. 2012, 134, 13708−13715

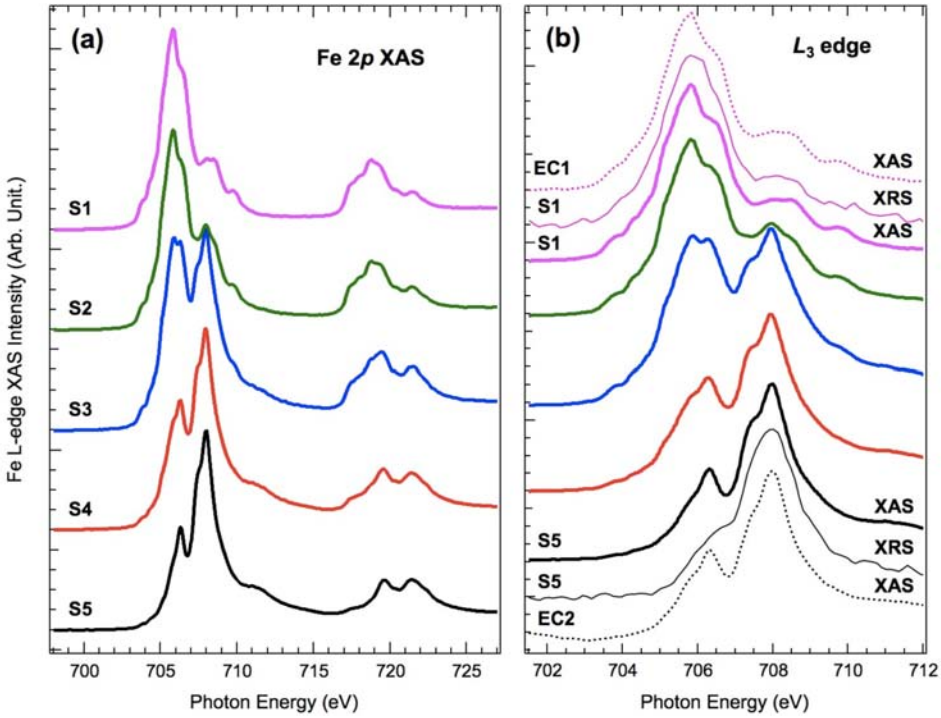


**Figure 1.** (a) Fe *L*-edge XAS of five chemically delithiated $Li_xFePO_4$ ($0 < x < 1$) nanorods. S5 is fully delithiated $FePO_4$,and S1 is $LiFePO_4$. (b) Fe-$L_3$ XAS spectra collected on chemically prepared S1−S5 samples (thicker solid line) and electrochemically prepared $LiFePO_4$ (EC1) and $FePO_4$ (EC2) samples (dotted lines). Hard XRS spectra of S1 and S5 are plotted as the thinner solid lines.

spectral line shape are intrinsically bulk properties, testifying that the discussed fine structures are not from any surface effect.

**DFT.** The first-principles calculation is based on the GGA+U approach[44] with the Perdew−Burke−Ernzerh of exchange−correlation functional[45] and projector augmented wave method[46] implemented in VASP.[47] Our DFT+U calculation follows the same approach described by Zhou et al.[30] The self-consistency of bulk calculation is done with a 4×4×8 *k*-point mesh. The kinetic energy cutoff is 550 eV. The value of Hubbard parameter *U* is 4.5 eV for $FePO_4$ and 3.71 eV for $LiFePO_4$. The effect of the *U* term is to drive the Fe 3d orbital occupation numbers to integer 0 or 1, favoring charge localization and consequently reproducing the phase separation into $Fe^{2+}$ and $Fe^{3+}$ compounds.

Charge-transfer multiplet calculations are performed with CTM4XAS program.[48] We calculated more than 9000 Fe-L edge XAS spectra for $LiFePO_4$ ($Fe^{2+}$) and $FePO_4$ ($Fe^{3+}$) with different ligand-field parameters: $0.4 < 10Dq < 1.2$ with 0.1 interval, $-0.3 < Ds < 0.3$ and $-0.3 < Dt < 0.3$ with 0.02 intervals. We then compared each individual simulation with the experimental data to find the optimized ligand-field parameters from the thousands of data sets.

## RESULTS AND DISCUSSION

**Soft X-ray Absorption and Hard X-ray Raman Spectroscopy.** For transition-metal (TM) compounds, soft X-ray spectroscopy directly probes the TM 3d valence states through dipole selection rules.[49] These are the most sensitive states to the electronic properties of the materials. We have demonstrated lately that the direct probe of such states in the vicinity of the Fermi level is critical for understanding and optimizing materials for battery applications.[50] In $Li_xFePO_4$, Fe 3d states are directly associated with the redox process in batteries and the local lattice distortions. The sensitivity provides abundant information on electronic structure that is relevant to battery performance, such as valency, spin states, and local structural effects on the crystal field.

Figure 1a shows the Fe *L*-edge XAS spectra of a series of $Li_xFePO_4$ samples at different chemical delithiation stages. Fe *L*-edge XAS involves the excitation of Fe 2p core electrons to the empty 3d orbitals. This dipole-allowed 2p-to-3d transition offers a direct probe of the Fe 3d electrons with high-intensity and minimum core−hole broadening. The spectra consist of sharp peaks, so-called white lines, in two regions, $L_3$ around 707 eV and $L_2$ around 720 eV, resulting from the core−hole spin−orbital coupling split. The overall line shape and the high-intensity ratio of the white line peaks[51] in Figure 1a suggests the high-spin states of the Fe 3d electrons, consistent with theoretical calculations and XPS results.[36]

In this work, we focus on the detailed line shape of the $L_3$ edge, as shown in Figure 1b. Overall, the $L_3$ edge features exhibit roughly two groups of peaks around 706 and 708 eV. For the two end members of $LiFePO_4$ and $FePO_4$, chemically and electrochemically prepared samples exhibit the same line shape, and the results are consistent with previous publications on chemically prepared samples.[37,38] The intensity ratio of these multiplet structures is a fingerprint of different oxidation states of iron,[52] i.e., $Fe^{2+}$ in $LiFePO_4$ and $Fe^{3+}$ in $FePO_4$. For the three intermediate states, the spectra compose of features corresponding to the contribution from both $LiFePO_4$ and $FePO_4$, as analyzed in detail below.

The soft XAS is a surface sensitive technique. In particular, the probing depth of TEY is typically several nanometers. Although with a probing depth of about two scales larger than TEY, TFY has recently been found to suffer serious spectral distortions in cathode materials without high-*Z* elements,[42] which defeats the purpose of this work on analyzing the details of the spectra. In order to verify that the fine structures in the spectra are intrinsic bulk properties, we performed the hard X-ray Raman measurements, whose process is principally analogous to the XAS but with a probe depth of several


dx.doi.org/10.1021/ja303225e | J. Am. Chem. Soc. 2012, 134, 13708−13715

micrometers. Fe-$L_3$ XRS spectra of $LiFePO_4$ (S1) and $FePO_4$ (S5) are shown as the thinner lines in Figure 1b. Although the resolution and statistics are not as high as that of soft X-ray spectra, it is clear that the XRS reproduced the line shape of the soft X-ray XAS spectra. This comparison of surface and bulk information confirms that the features in the spectra that will be elaborated in this work are not due to surface effects, e.g., variation of surface oxidation states or surface contamination. Such verification, although important, has not been performed before.

**Two-Phase Simulations.** As shown in Figure 1, the line shape of the $L_3$ edge varies systematically and shows a monotonic evolution upon delithiation. The abundant fine structures in the spectra enable a quantitative test of the two-phase model. In general, Figure 2a,b displays all the spectra of

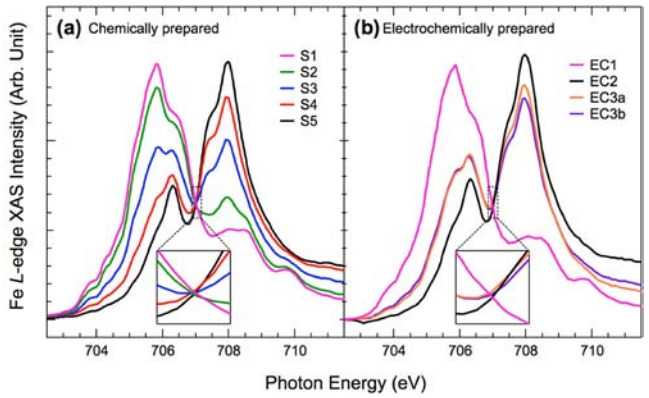


**Figure 2.** Isosbestic point of chemical delithiation samples (a) and electrochemically cycled samples (b).

the chemically (S1−5) and electrochemically (EC1−3) delithiated samples, respectively. The spectra are all normalized to the total area of the Fe-$L_3$ features shown in Figure 2. Both plots show the isosbestic point of all the spectra (insets of Figure 2a,b) but with slight deviation in the electrochemically prepared samples. Such isosbestic points indicate the dominating two-phase transformation upon (de)lithiation.

In Figure 3a−e, we construct the simulated spectra for intermediate states by linear combinations of the spectra of the two end states, i.e., following the two-phase scenario. The best fitting results of chemically delithiated samples S2−S4, shown as the solid lines in Figure 3a−c, almost completely overlap with the experimental data. All the fine structures can be precisely reconstructed. This perfect fitting is another proof of the validity of the two-phase model for these samples, from a spectroscopic point of view. The fittings for three intermediate states are equivalent to $Li_{0.84}FePO_4$, $Li_{0.48}FePO_4$, and $Li_{0.19}FePO_4$, respectively, with fitting precisions within 0.001 of the Li content. This method by linear combination of two end-state components was also employed before in the EELS[15] and X-ray studies[39] but with much less precision due to the resolution issue.

The high-quality spectroscopic data not only provide another precise and objective way to determine the (de)lithiation level, but also enable a more sensitive approach to studying the subtle effects in the two-phase issue. Contrasting the perfect isosbestic point (Figure 2a) and the two-phase fitting (Figure 3a−c) of the data collected on S1−5 samples, the spectra from the electrochemically delithiated samples display weak but consistent deviation from the same type of fitting. Figure 3d,e shows the Fe-$L_3$ XAS of electrochemically cycled $Li_xFePO_4$ cathode, EC3. Two sides of the cathode, one facing the electrolyte and the other facing the current collector, were measured separately. The two-phase fitting, although good overall, cannot be achieved as perfectly as those for samples S2−4 shown in Figure 3a−c, which can be seen as the consistent deviation around 707.5 eV with different spectral normalization and multiple tests. The difference between the two-phase fitting and experimental spectra is about 2-fold larger in these samples (Figure 3f). As the 707.5 eV is clearly offset from the highest intensity peak (red arrows), this deviation is not simply due to systematic error that yields the strongest effect at the highest intensity. The even worse fitting at higher energy (>709 eV) is due to the background signal from the multiple components in the electrochemically prepared samples, e.g., binder and conductive additives. As the sign of such background contribution is opposite to the discussed difference around 707.5 eV, it does not invalidate the weak deviation from two-phase configuration, which is actually stronger if one normalizes out the background contribution.

The subtle deviation from the two-phase fitting in the electrochemically delithiated samples is a nontrivial discovery. While both our overall spectral line shape (Figure 2) and the electron microscopic data confirm the predominant two-phase in these samples,[17] the very weak spectral deviation from two-phase fitting naturally corresponds to an intermediate phase within a very limited region, i.e., the phase boundary, instead of a bulk solid−solution phase.[53−55] Therefore, the contrast between chemically and electrochemically prepared samples more likely stems from the intrinsic formation of such a boundary phase,[8,18] instead of other factors, like particle size, temperature, or synthesis conditions. Additionally, the contrast on this subtle deviation between EC3a,b and S2−S4 samples indicates that the electrochemical process may be more inclined to form such a boundary phase, and the data is consistent with the theoretical speculation that such a phase is kinetically driven metastable.[11] The demonstrated sensitivity of the high-resolution soft X-ray data enables an important nonstructural approach for studying the decay and forming of this critical phase, which is currently in process.

Another reproducible observation, based on the fitting parameters, is that the line shape of the spectra yields slightly different Li concentrations on the two opposite sides of the cathode. There is more $Fe^{2+}$ ($LiFePO_4$) component (29%) on the side facing the current collector than the other side facing the electrolyte (25%), which reflects the lateral distribution gradient of Li in the cathodes caused by the electrodes' spacial polarization, which is consistent with previous findings.[56] Soft X-ray spectroscopy provides another sensitive probe of the overall Li gradient produced during electrochemical cycling.

**DFT Calculation.** In order to deliver a complete picture of the (de)lithiation effect on electronic structure of this system, we performed two types of theoretical calculations to resolve the multiple features in our spectra. First, the partial DOS (pDOS) of $LiFePO_4$ and $FePO_4$ have been calculated with GGA+U, which has been successfully applied for calculating the electronic structure of cathode materials before.[29,30]

The GGA+U calculation of the pDOS of Fe 3d is shown in Figure 4a,b. The octahedral distortions calculated within DFT +U are in very good agreement with available structural data.[25,57] In general, the quasi-octahedral local structure around the Fe determines a crystal field potential, which splits the five 3d states into two groups: $T_{2g}$ (3-fold) and $E_g$ (2-fold). It is


dx.doi.org/10.1021/ja303225e | J. Am. Chem. Soc. 2012, 134, 13708−13715

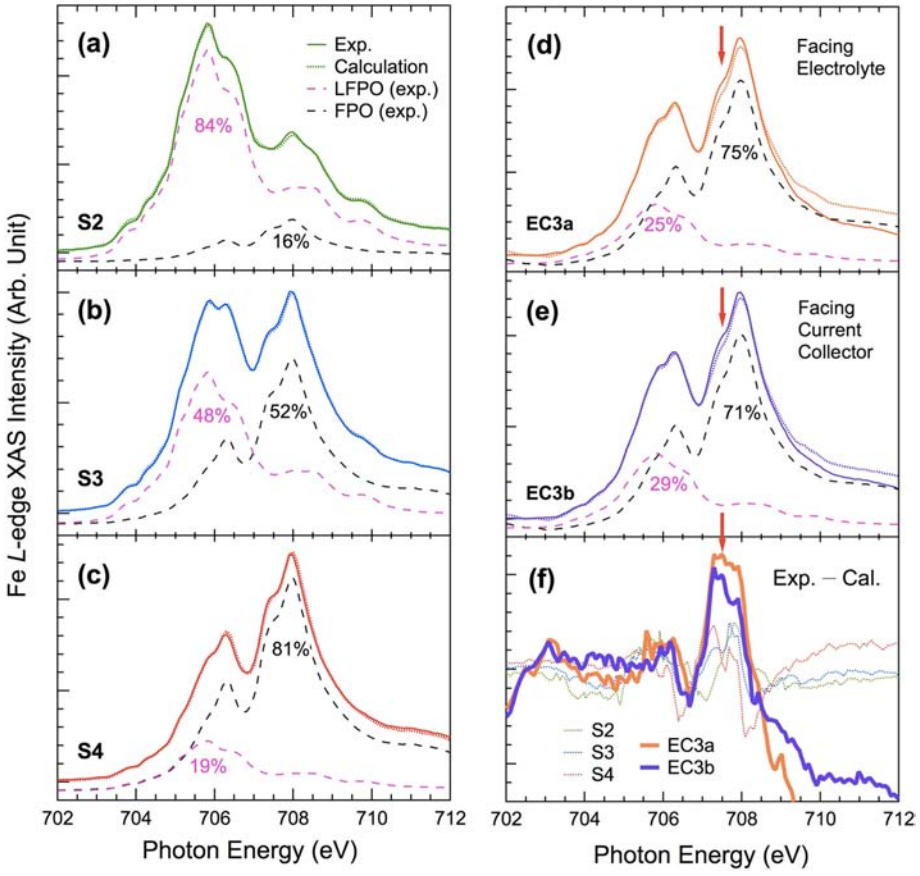


**Figure 3.** (a–c) Comparison of the experimental (solid lines) and two-phase fitting spectra (dot lines) of three partially chemically delithiated $Li_xFePO_4$: S2–S4. (d,e) Same comparison of partially electrochemically cycled $Li_xFePO_4$ cathode facing electrolyte (EB3a) and current collector side (EB3b). (f) Difference between experimental and two-phase fitting spectra of the electrochemically (thick lines) and chemically (thin lines) samples.

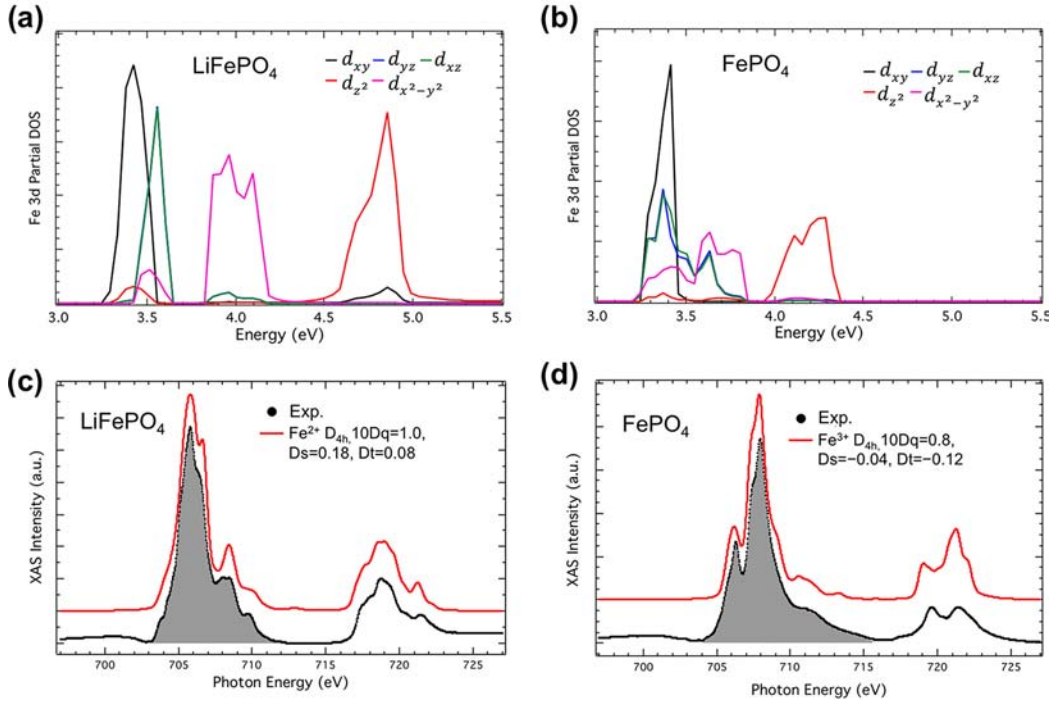


**Figure 4.** Fe 3d unoccupied partial DOS of $LiFePO_4$ (a) and $FePO_4$ (b) calculated by GGA+U method. The zero of the energy axis is arbitrary and has been chosen to roughly align the DOS for easy comparison. Ligand field multiplet simulations (red curves) are compared to the experimental Fe *L*-edge XAS (black dots) of $LiFePO_4$ (c) and $FePO_4$ (d).


dx.doi.org/10.1021/ja303225e | *J. Am. Chem. Soc.* 2012, 134, 13708–13715

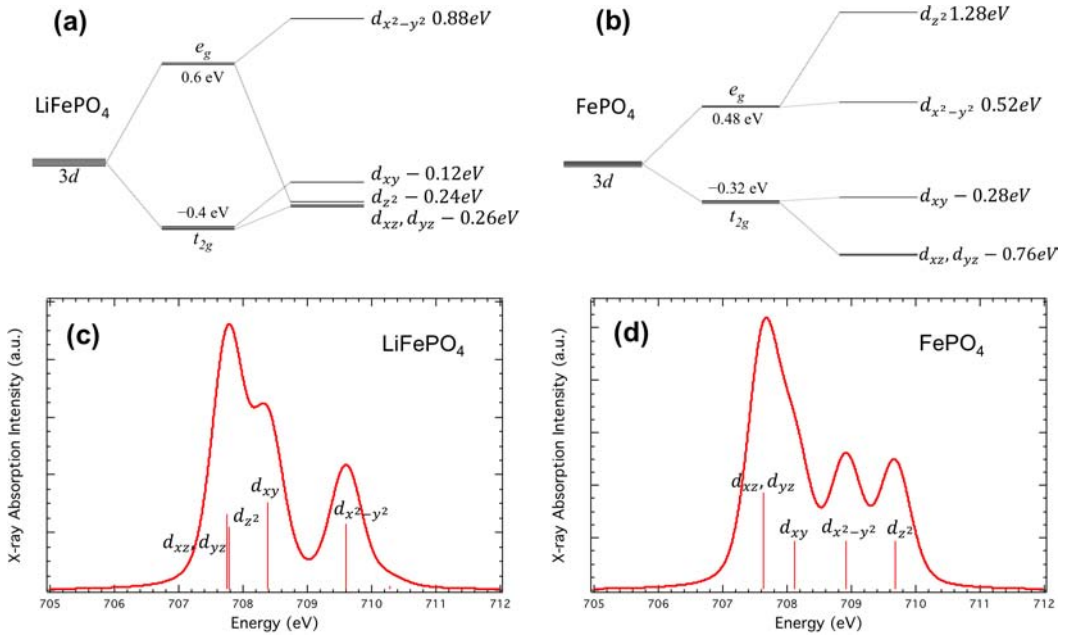


**Figure 5.** (a,b) Crystal field diagram of $LiFePO_4$ (a) and $FePO_4$ (b) derived from the multiplet calculations. (c,d) Theoretical calculations for $LiFePO_4$ (c) and $FePO_4$ (d) with exactly the same crystal field parameters used in Figure 4c,d but without the multiplet effect from 2p−3d overlap.

obvious that the overall 3d states of $LiFePO_4$ are more isolated than those of $FePO_4$. This implies that the system becomes more ionic after lithiation. The calculated pDOS also qualitatively defines that the energy splitting of the $T_{2g}$ and $E_g$ states ($10Dq$) is of the order of 1 eV.

**Ligand Field Multiplet Calculations.** Typically, the DFT DOS cannot be directly observed in the TM *L*-edge X-ray absorption spectra because of the strong overlap of core and valence wave functions, the so-called multiplet effect. In order to simulate our experimental data and get detailed information on the electronic structure, we carried out Fe *L*-edge XAS simulations using ligand field multiplet theory,[48,49] which describes the transition for a single Fe ion from a $3d^n$ ground state to $\underline{2p}3d^{n+1}$ final state. In multiplet calculation, the molecular environment and local symmetry are described using a ligand field potential. When the symmetry is lowered from octahedral $O_h$ to $D_{4h}$, the separated $T_{2g}$ and $E_g$ states are further split by two ligand field parameters *Ds* and *Dt*. The crystal field levels (i.e., the energy of 3d orbitals) can be derived as: $d_{x^2-y^2} = 6Dq + 2Ds - 1Dt$, $d_{z^2} = 6Dq - 2Ds - 6Dt$, $d_{xy} = -4Dq + 2Ds - 1Dt$, $d_{xz} = d_{yz} = -4Dq - 1Ds + 4Dt$. Therefore, the multiplet calculations, by comparison with experimental data, will be able to deliver a complete set of parameters that defines the evolution of electronic structure affected by the local lattice distortion.

The comparison of the 9000 simulated spectra with our experimental data yielded the best multiplet simulations of $LiFePO_4$ and $FePO_4$ shown in Figure 4c,d. The crystal field parameters are $10Dq = 1.0$, $Ds = 0.18$, $Dt = 0.08$ for $LiFePO_4$ and $10Dq = 0.8$, $Ds = -0.04$, $Dt = -0.12$ for $FePO_4$. The simulations are in excellent agreement with the experiments. The overall line shape, positions, and intensities of the main features are correctly reproduced.

**Fe 3d Reconfiguration.** From the combined theoretical and experimental investigation, we now discuss quantitatively the impact of the (de)lithiation on the Fe 3d states through the local distortions in the $LiFePO_4$ system. The corresponding Fe 3d crystal field diagrams of $LiFePO_4$ and $FePO_4$ are plotted in Figure 5a,b. Besides the quantitative variation on all the energy levels, the $d_{z^2}$ state (highlighted in red) has been lowered in $LiFePO_4$. This effect is intuitively understandable by considering the elongated *z*-axis of the $FeO_6$ octahedron in $LiFePO_4$, consistent with the structural studies.[25,57]

In order to assign the XAS spectral features to particular Fe 3d states, we further performed the calculation by turning off the atomic 2p−3d overlap (the multiplet effect), as demonstrated successfully before.[58] In Figure 5c,d, the Fe-$L_3$ spectra of $LiFePO_4$ and $FePO_4$ are calculated with the same crystal field parameters shown in Figure 4c,d, however, without multiplet effects. Although the energy, line shape, and features of these calculated spectra cannot be directly compared with the experimental data, they qualitatively pinpoint the relative position of the five Fe 3d orbitals.[58] In particular for $LiFePO_4$, the $d_{xy}$ orbital is situated above the degenerated $d_{xz}/d_{yz}$ and the $d_{z^2}$ states.

**Anisotropic Electronic Structure in $LiFePO_4$ Single Crystals.** Experimentally, to directly identify the simulated Fe 3d state, configuration is a nontrivial problem. It requires a technique that can distinguish the 3d states. Here we tackle this issue through polarization-dependent soft X-ray spectroscopy on $LiFePO_4$ single crystals. Our particular concentration is on the direction of the one-dimensional lithium diffusion,[19−22] i.e., the *b*-axis along [010] in Figure 6b. The $LiFePO_4$ single crystal was thus cut along *b*/*c* plane. The linearly polarized soft X-ray beam was carefully aligned to hit the azimuthal rotation center of the sample. The variation of X-ray polarization, in respect of the crystal lattice, is the only changing experimental parameter for catching reliable polarization-dependent information.

When the electric field vector *E* is along the lithium diffusion direction, *b*-axis, the most striking polarization dependence, as shown in Figure 6a, is the much-enhanced 707 eV feature. The TFY spectra of the single crystal, which somehow do not suffer serious line shape distortion as in the nanoparticle samples,[42] display the same anisotropic effect (inset), ruling out any surface effect for this phenomenon.


dx.doi.org/10.1021/ja303225e | J. Am. Chem. Soc. 2012, 134, 13708−13715

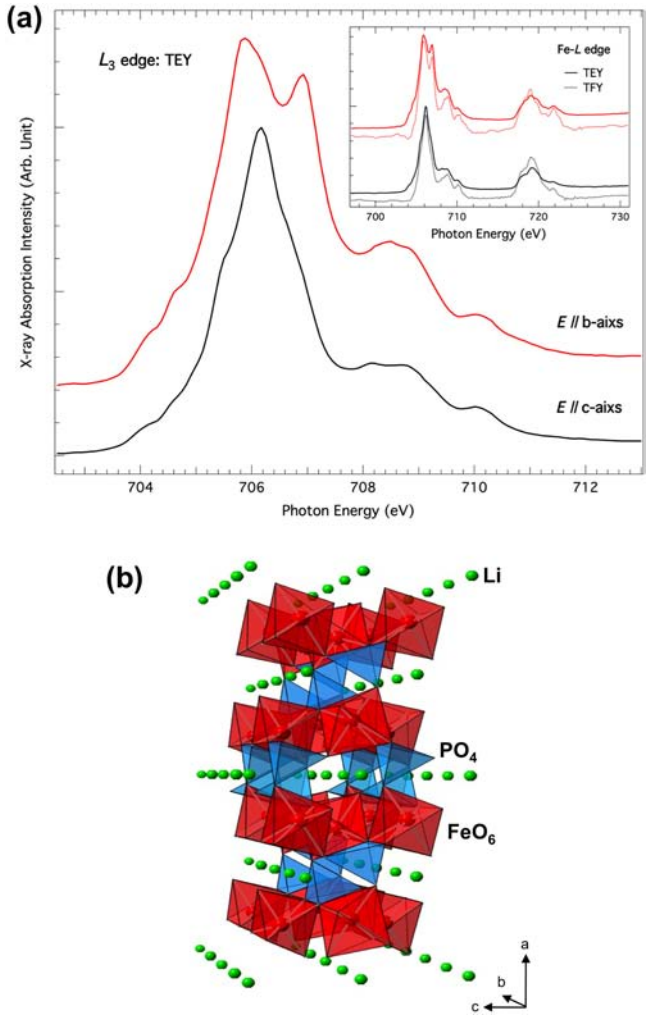


**Figure 6.** (a) Fe-$L_3$ TEY XAS spectra of $LiFePO_4$ single crystal obtained for the electric field vector along the *b*-axis (red) and *c*-axis (black), respectively. Both TEY (solid lines) and TFY (dotted lines) spectra over the entire *L*-edge are shown in the inset. (b) Crystal structure of $LiFePO_4$.

The crystal structure of $LiFePO_4$ (Figure 6b) comprises the $FeO_6$ octahedra (in red) interwoven with the $PO_4$ tetrahedra (in blue). Corner-sharing $FeO_6$ octahedra build up two-dimensional buckled sheets in the *bc* plane. The directions of the Fe 3d orbitals are not exactly along the directions of the three lattice axes. However, the $d_{xy}$ orbital is aligned approximately to the lattice *b*-axis. According to the dipole approximation for soft XAS,[49] the strongly enhanced 707 eV peak should correspond to the Fe $3d_{xy}$ orbital. This experimental assignment is indeed consistent with the 3d state configurations shown in the crystal field calculation of $LiFePO_4$ (Figure 5c).

Finally, we would like to note that the observed enhancement of the Fe $3d_{xy}$ state, with the electric field along the lithium diffusion direction, provides new electronic structure insight for understanding the anisotropic electric and ionic transport in $LiFePO_4$, which are strongly coupled together in this system.[9]

## CONCLUSION

Through a combination of high-resolution spectroscopy and theory, we systematically studied the (de)lithiation effects on electronic structure in chemically and electrochemically prepared $Li_xFePO_4$. The soft X-ray Fe *L*-edge spectra fingerprint the (de)lithiation process. Two-phase fittings of the spectra are consistent with an overall two-phase transformation, providing precise information on lithium composition and distribution gradient across the electrode. More importantly, from the electronic structure point of view, the two-phase fitting of high-quality spectra allows us to detect the subtle deviation from two-phase behavior. The observed small deviation indicates the existence of a finite amount of a nonequilibrium intermediate phase instead of a bulk solid–solution phase. This result provides crucial experimental evidence for the (de)lithiation model based on the kinetics of metastable boundary phases in $Li_xFePO_4$ system.[8,11,18]

From the detailed line shape of the spectra, we are also able to derive quantitatively the evolution of the 3d state configuration upon (de)lithiation of $Li_xFePO_4$ by performing both first-principles calculations and multiplet simulations. The crystal field potential from the GGA+U calculation agrees qualitatively with that of the multiplet simulations of our experimental spectra, providing a fundamental support of the more empirical multiplet approach.

In order to experimentally verify the derived 3d states, we further measured $LiFePO_4$ single crystals with different X-ray polarization directions. The polarization-dependent spectra show an intriguing enhancement of the Fe $3d_{xy}$ state along *b*-axis, the lithium diffusion direction. This anisotropic electronic structure, which was only studied indirectly before, is consistent with our 3d state definition and also provides new electronic structure information for understanding the inherent anisotropic nature of lithium diffusion and electron conduction.

Our analysis provides systematic and in-depth information on the interplay between (de)lithiation process of $Li_xFePO_4$ and its electronic structure. The study provides experimental verification and regulation for theoretical calculations. The new information on phase transformation, Li distribution, and strongly anisotropic electron states sheds light on understanding the puzzles of the (de)lithiation and transport mechanisms in the $LiFePO_4$ system.

## ASSOCIATED CONTENT

### Supporting Information

Typical TEM images and XRD patterns of chemically prepared $Li_xFePO_4$ nanorods and synchrotron-based XRD of $LiFePO_4$ single crystals. This material is available free of charge via the Internet at http://pubs.acs.org.

## AUTHOR INFORMATION

### Corresponding Author

WLYang@lbl.gov

### Notes

The authors declare no competing financial interest.

## ACKNOWLEDGMENTS

We are grateful to Philip Ross and Matteo Cococcioni for useful discussions. This work is supported by the LDRD program at the Lawrence Berkeley National Laboratory. The Advanced Light Source (ALS) is supported by the U.S. Department of Energy under contract no. DE-AC03-76SF00098. The work at Northeastern University is supported by the U.S. Department of Energy under contract no. DE-FG02-07ER46352 and benefitted from allocation of computer

time at the NERSC and NU-ASCC computation centers. The Stanford Synchrotron Radiation Lightsource is operated by Stanford University on behalf of the U.S. Department of Energy, Office of Basic Energy Sciences.

## REFERENCES

(1) Tarascon, J. M.; Armand, M. *Nature* **2001**, *414*, 359.
(2) Armand, M.; Tarascon, J. M. *Nature* **2008**, *451*, 652.
(3) Tarascon, J. M. *Philos. Trans. R. Soc., A* **2010**, *368*, 3227.
(4) Padhi, A. K.; Nanjundaswamy, K. S.; Goodenough, J. B. *J. Electrochem. Soc.* **1997**, *144*, 1188.
(5) Padhi, A. K.; Nanjundaswamy, K. S.; Masquelier, C.; Okada, S.; Goodenough, J. B. *J. Electrochem. Soc.* **1997**, *144*, 1609.
(6) Chung, S. Y.; Bloking, J. T.; Chiang, Y. M. *Nat. Mater.* **2002**, *1*, 123.
(7) Chung, S. Y.; Chiang, Y. M. *Electrochem. Solid-State Lett.* **2003**, *6*, A278.
(8) Chen, G.; Song, X.; Richardson, T. J. *Electrochem. Solid-State Lett.* **2006**, *9*, A295.
(9) Ellis, B.; Perry, L. K.; Ryan, D. H.; Nazar, L. F. *J. Am. Chem. Soc.* **2006**, *128*, 11416.
(10) Li, J.; Yao, W.; Martin, S.; Vaknin, D. *Solid State Ionics* **2008**, *179*, 2016.
(11) Malik, R.; Zhou, F.; Ceder, G. *Nat. Mater.* **2011**, *10*, 587.
(12) Morgan, D.; Van der Ven, A.; Ceder, G. *Electrochem. Solid-State Lett.* **2004**, *7*, A30.
(13) Zaghib, K.; Mauger, A.; Goodenough, J. B.; Gendron, F.; Julien, C. M. *Chem. Mater.* **2007**, *19*, 3740.
(14) Andersson, A. S.; Kalska, B.; Haggstrom, L.; Thomas, J. O. *Solid State Ionics* **2000**, *130*, 41.
(15) Laffont, L.; Delacourt, C.; Gibot, P.; Wu, M. Y.; Kooyman, P.; Masquelier, C.; Tarascon, J. M. *Chem. Mater.* **2006**, *18*, 5520.
(16) Yamada, A.; Koizumi, H.; Nishimura, S. I.; Sonoyama, N.; Kanno, R.; Yonemura, M.; Nakamura, T.; Kobayashi, Y. *Nat. Mater.* **2006**, *5*, 357.
(17) Gu, L.; Zhu, C.; Li, H.; Yu, Y.; Li, C.; Tsukimoto, S.; Maier, J.; Ikuhara, Y. *J. Am. Chem. Soc.* **2011**, *133*, 4661.
(18) Suo, L.; Han, W.; Lu, X.; Gu, L.; Hu, Y.-S.; Li, H.; Chen, D.; Chen, L.; Tsukimoto, S.; Ikuhara, Y. *Phys. Chem. Chem. Phys.* **2012**, *14*, 5363.
(19) Morgan, D.; Ven, A. V. d.; Ceder, G. *Electrochem. Solid-State Lett.* **2004**, *7*, A30.
(20) Islam, M. S.; Driscoll, D. J.; Fisher, C. A. J.; Slater, P. R. *Chem. Mater.* **2005**, *17*, 5085.
(21) Nishimura, S.-i.; Kobayashi, G.; Ohoyama, K.; Kanno, R.; Yashima, M.; Yamada, A. *Nat. Mater.* **2008**, *7*, 707.
(22) Amin, R.; Balaya, P.; Maier, J. *Electrochem. Solid-State Lett.* **2007**, *10*, A13.
(23) Maxisch, T.; Zhou, F.; Ceder, G. *Phys. Rev. B* **2006**, *73*, 104301.
(24) Ong, S. P.; Chevrier, V. L.; Ceder, G. *Phys. Rev. B* **2011**, *83*, 075112.
(25) Liang, G.; Park, K.; Li, J.; Benson, R. E.; Vaknin, D.; Markert, J. T.; Croft, M. C. *Phys. Rev. B* **2008**, *77*, 064414.
(26) Shi, S.; Ouyang, C.; Xiong, Z.; Liu, L.; Wang, Z.; Li, H.; Wang, D.-s.; Chen, L.; Huang, X. *Phys. Rev. B* **2005**, *71*, 144404.
(27) Tang, P.; Holzwarth, N. A. W. *Phys. Rev. B* **2003**, *68*, 165107.
(28) Xu, Y. N.; Chung, S. Y.; Bloking, J. T.; Chiang, Y. M.; Ching, W. Y. *Electrochem. Solid-State Lett.* **2004**, *7*, A131.
(29) Zhou, F.; Kang, K. S.; Maxisch, T.; Ceder, G.; Morgan, D. *Solid State Commun.* **2004**, *132*, 181.
(30) Zhou, F.; Marianetti, C. A.; Cococcioni, M.; Morgan, D.; Ceder, G. *Phys. Rev. B* **2004**, *69*, 201101.
(31) Ouyang, C.; Shi, S.; Wang, Z.; Huang, X.; Chen, L. *Phys. Rev. B* **2004**, *69*, 104303.
(32) Seo, D.; Gwon, H.; Kim, S.; Kim, J.; Kang, K. *Chem. Mater.* **2010**, *22*, 518.
(33) Miao, S.; Kocher, M.; Rez, P.; Fultz, B.; Yazami, R.; Ahn, C. C. *J. Phys. Chem. A* **2007**, *111*, 4242.
(34) Sigle, W.; Amin, R.; Weichert, K.; van Aken, P. A.; Maier, J. *Electrochem. Solid-State Lett.* **2009**, *12*, A151.
(35) Kinyanjui, M. K.; Axmann, P.; Wohlfahrt-Mehrens, M.; Moreau, P.; Boucher, F.; Kaiser, U. *J. Phys.: Condens. Matter* **2010**, *22*, 275501.
(36) Castro, L.; Dedryvere, R.; El Khalifi, M.; Lippens, P.; Breger, J.; Tessier, C.; Gonbeau, D. *J. Phys. Chem. C* **2010**, *114*, 17995.
(37) Augustsson, A.; Zhuang, G. V.; Butorin, S. M.; Osorio-Guillen, J. M.; Dong, C. L.; Ahuja, R.; Chang, C. L.; Ross, P. N.; Nordgren, J.; Guo, J. H. *J. Chem. Phys.* **2005**, *123*, 184717.
(38) Hunt, A.; Ching, W. Y.; Chiang, Y. M.; Moewes, A. *Phys. Rev. B* **2006**, *73*, 205120.
(39) Wang, X.-J.; Jaye, C.; Nam, K.-W.; Zhang, B.; Chen, H.-Y.; Bai, J.; Li, H.; Huang, X.; Fischer, D. A.; Yang, X.-Q. *J. Mater. Chem.* **2011**, *21*, 11406.
(40) Yang, S.; Wang, D.; Liang, G.; Yiu, Y. M.; Wang, J.; Liu, L.; Sun, X.; Sham, T.-K. *Energy Environ. Sci.* **2012**, *5*, 7007.
(41) Deb, A.; Bergmann, U.; Cramer, S. P.; Cairns, E. J. *Electrochim. Acta* **2005**, *50*, 5200.
(42) Wadati, H.; Achkar, A. J.; Hawthorn, D. G.; Regier, T. Z.; Singh, M. P.; Truong, K. D.; Fournier, P.; Chen, G.; Mizokawa, T.; Sawatzky, G. A. *Appl. Phys. Lett.* **2012**, *100*, 193906.
(43) Sokaras, D.; N., D.; Weng, T.-C.; Alonso-Mori, R.; Velikov, P.; Wenger, D.; Garachtchenko, A.; George, M.; Borzenets, V.; Johnson, B.; Qian, Q.; Rabedeau, T.; Bergmann, U. *Rev. Sci. Instrum.* **2012**, *83*, 043112.
(44) Dudarev, S. L.; Botton, G. A.; Savrasov, S. Y.; Humphreys, C. J.; Sutton, A. P. *Phys. Rev. B* **1998**, *57*, 1505.
(45) Kresse, G.; Joubert, D. *Phys. Rev. B* **1999**, *59*, 1758.
(46) Blochl, P. E. *Phys. Rev.* **1994**, *B50*, 17953.
(47) Kresse, G.; Furthmuller, J. *Comput. Mater. Sci.* **1996**, *6*, 15.
(48) Stavitski, E.; de Groot, F. M. F. *Micron* **2010**, *41*, 687.
(49) de Groot, F.; Kotani, A. *Core level spectroscopy of solids*; CRC Press: Boca Raton, FL, 2008.
(50) Liu, G.; Xun, S.; Vukmirovic, N.; Song, X.; Olalde-Velasco, P.; Zheng, H.; Battaglia, V. S.; Wang, L.; Yang, W. *Adv. Mater.* **2011**, *23*, 4679.
(51) Thole, B. T.; van der Laan, G. *Phys. Rev. B* **1988**, *38*, 3158.
(52) Cook, P. L.; Liu, X. S.; Yang, W. L.; Himpsel, F. J. *J. Chem. Phys.* **2009**, *131*, 194701.
(53) Chen, G.; Song, X.; Richardson, T. J. *J. Electroche. Soc.* **2007**, *154*, A627.
(54) Ellis, B. L.; Lee, K. T.; Nazar, L. F. *Chem. Mater.* **2010**, *22*, 691.
(55) Meethong, N.; Huang, H.-Y. S.; Carter, W. C.; Chiang, Y.-M. *Electrochem. Solid-State Lett.* **2007**, *10*, A134.
(56) Liu, J.; Kunz, M.; Chen, K.; Tamura, N.; Richardson, T. J. *J. Phys. Chem. Lett.* **2010**, *1*, 2120.
(57) Delmas, C.; Maccario, M.; Croguennec, L.; Le Cras, F.; Weill, F. *Nat. Mater.* **2008**, *7*, 665.
(58) Amin, R.; Balaya, P.; Maier, J. *Electrochem. Solid-State Lett.* **2007**, *10*, A13.